

Water permeability of nanoporous graphene at realistic pressures for reverse osmosis desalination

David Cohen-Tanugi and Jeffrey C. Grossman

Citation: *The Journal of Chemical Physics* **141**, 074704 (2014); doi: 10.1063/1.4892638

View online: <http://dx.doi.org/10.1063/1.4892638>

View Table of Contents: <http://scitation.aip.org/content/aip/journal/jcp/141/7?ver=pdfcov>

Published by the [AIP Publishing](#)

Articles you may be interested in

Erratum: "Water permeability of nanoporous graphene at realistic pressures for reverse osmosis desalination" [*J. Chem. Phys.* **141**, 074704 (2014)]

J. Chem. Phys. **141**, 119901 (2014); 10.1063/1.4896215

Mechanical properties of nanoporous graphene membrane

J. Appl. Phys. **115**, 034303 (2014); 10.1063/1.4862312

Water permeation through single-layer graphyne membrane

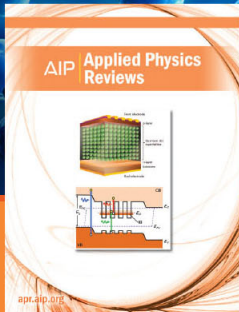
J. Chem. Phys. **139**, 064705 (2013); 10.1063/1.4817596

Zeolitic imidazolate framework-8 as a reverse osmosis membrane for water desalination: Insight from molecular simulation

J. Chem. Phys. **134**, 134705 (2011); 10.1063/1.3573902

Reverse osmosis desalination: Modeling and experiment

Appl. Phys. Lett. **94**, 124102 (2009); 10.1063/1.3109795



NEW Special Topic Sections

NOW ONLINE
Lithium Niobate Properties and Applications:
Reviews of Emerging Trends

AIP | Applied Physics
Reviews

Water permeability of nanoporous graphene at realistic pressures for reverse osmosis desalination

David Cohen-Tanugi and Jeffrey C. Grossman

Department of Materials Science and Engineering, Massachusetts Institute of Technology, Cambridge, Massachusetts 02139, USA

(Received 2 June 2014; accepted 29 July 2014; published online 18 August 2014)

Nanoporous graphene (NPG) shows tremendous promise as an ultra-permeable membrane for water desalination thanks to its atomic thickness and precise sieving properties. However, a significant gap exists in the literature between the ideal conditions assumed for NPG desalination and the physical environment inherent to reverse osmosis (RO) systems. In particular, the water permeability of NPG has been calculated previously based on very high pressures (1000–2000 bars). Does NPG maintain its ultrahigh water permeability under real-world RO pressures (<100 bars)? Here, we answer this question by drawing results from molecular dynamics simulations. Our results indicate that NPG maintains its ultrahigh permeability even at low pressures, allowing a permeate water flux of 6.0 l/h-bar per pore, or equivalently $1041 \pm 20 \text{ l/m}^2\text{-h-bar}$ assuming a nanopore density of $1.7 \times 10^{13} \text{ cm}^{-2}$. © 2014 AIP Publishing LLC. [<http://dx.doi.org/10.1063/1.4892638>]

I. INTRODUCTION

Water desalination is expected to play an increasingly crucial role in the challenge to supply enough clean water in the 21st century.¹ While reverse osmosis (RO) remains the most energy-efficient desalination method,² the RO membranes that are required for separating salts and other molecular species from water exhibit low water permeability, i.e., a low water flux per unit of applied pressure. In particular, if RO membranes were $3\times$ more permeable for the same salt rejection, desalination plants could operate at 46% lower pressure or 270% greater permeate production per vessel for brackish water.³ However, new membrane materials are needed before this benefit can be realized.

Nanostructured materials offer the promise of increased membrane permeability for more affordable and efficient water desalination.^{4–8} In particular, we predicted previously that nanoporous graphene (NPG) would reject salt ions with 2–3 orders of magnitude higher water permeability than conventional RO membranes.⁹ However, previous studies employed pressures that are several orders of magnitude higher (1000–2000 bars) than those in real RO systems (10–100 bars) in order to reduce computational time. Moreover, published studies have kept the atoms in the NPG membrane frozen in order to decouple the desalination performance from mechanical effects. However, graphene membranes synthesized experimentally are flexible and the functional groups at the edge of each nanopore are prone to deformation under the influence of water molecules and salt ions, which may in turn affect the permeability and salt rejection of the membrane.

In this work, we investigate whether NPG maintains its ultra-high permeability at the pressures employed in RO systems. Using classical MD simulations, we demonstrate that the permeability of NPG remains approximately constant down to very low pressures. We also show that NPG maintains its desalination performance even

when the flexibility of the membrane atoms is taken into account.

II. METHODS

The system was built and analyzed using Visual Molecular Dynamics (VMD) v1.9, and MD calculations were performed using the LAMMPS code (Figure 1).^{10,11} Saltwater at an osmotic pressure of 5.8 bars was generated on the feed side (i.e., the input side) of an NPG membrane, and consisted of 955 water molecules and 2 Na^+/Cl^- pairs, corresponding to a feed osmotic pressure of 5.8 bars according to the Morse equation. Likewise, 526 molecules of pure water were placed on the permeate side (i.e., the output side), and a rigid piston was placed on either side of the water in order to apply any desired transmembrane pressure.

Because we found previously that hydrogenated nanopores allow for higher salt rejection and that a pore radius of 0.7 nm allows for optimal water passage given the constraint of full salt rejection,⁹ we chose hydrogenated NPG with an open pore area of 23 \AA^2 in this work. The detailed methodology builds upon that of our previous work,⁹ although in the present work the membrane was allowed to deform during the simulation. The system was subjected to periodic boundary conditions in the x - and y -directions, and we used rigid pistons on either side of the system to control the transmembrane pressure in the z -direction. Forces on C and H atoms in the membrane were described with the AIREBO potential with a scale factor of 3.0.¹² One carbon atom was tethered to its original position in order to simulate the effect of a substrate that would prevent the entire membrane from moving out of plane. Forces on water molecules were described with the TIP4P model,¹³ which has been shown to accurately reproduce the entropic and hydrogen bonding behavior of liquid water.¹⁴ Interactions between water and carbon atoms were modeled with Lennard-Jones parameters using the Lorentz-Berthelot mixing rules. We

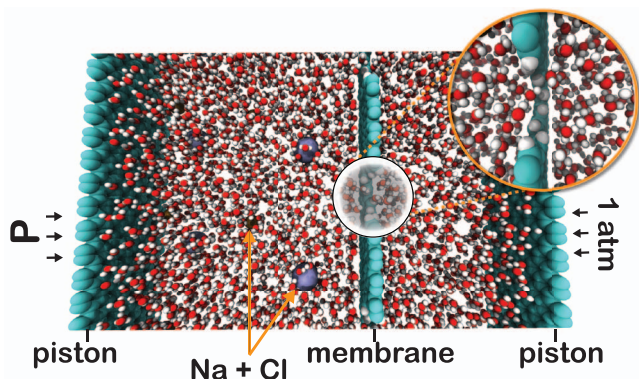


FIG. 1. Schematic of the computational setup. Salt water (NaCl) and pure water are placed on either side of a hydrogenated NPG membrane with $r = 0.7$ nm. Membrane atoms are allowed to move, and transmembrane pressure is applied using two pistons that exert pressures P and 1 atm on the feed and permeate side, respectively. The inset shows the permeation of water molecules across a nanopore.

used the pppm/tip4p k-space solver in LAMMPS with a precision of 10^{-6} . In addition, a time step of 0.5 fs was used in order to guarantee energy conservation to within numerical precision.

The saltwater and membrane were first subjected to a static minimization. Following minimization, the saltwater system was equilibrated for 50 ps in the NVT ensemble between the two pistons, each of which had a force of 0.01 kcal/mol/Å in order to bring the density of water to its equilibrium value and remove any voids in the liquid water. The data acquisition stage was performed in the NVT ensemble with a Nosé-Hoover thermostat and a damping constant of 100 ps. The choice of thermodynamic ensemble and thermostat has been shown to influence the water flowrates through carbon nanotubes, and the Nosé-Hoover thermostat is known to provide an underestimate of water permeability relative to other thermostat choices.¹⁵ Thus, the permeabilities reported here are conservative estimates. Water pressures on either side of the membrane were enforced by applying constant forces in the z -direction to the piston atoms, thus ensuring that both water reservoirs were kept at constant pressures. During the data acquisition stage, the permeate piston was assigned a new pressure of $P_p = 1$ atm and the feed piston was assigned a larger pressure P that varied for each simulation. Because $P \gg 1$ atm, the transmembrane pressure $\Delta P = P - P_p$ is approximately equal to P . The net driving pressure is $(\Delta P - \Delta \Pi) = (P - P_p) - (\pi_f - \pi_p)$, where $\Delta \Pi$ is the total osmotic pressure difference and π_f and π_p are the feed and permeate osmotic pressures, respectively. The data acquisition stage lasted 10 ns and atomic trajectories were recorded every 10 000 steps. Simulations were carried out for multiple values of P between 0 and 2400 bars. For each choice of P , the simulation was run 5–15 times with different and uncorrelated starting configurations in order to produce more accurate averages. The water flux, ϕ , across the membrane was computed as

$$\phi = \dot{N}v\rho, \quad (1)$$

where \dot{N} is the average rate of water molecules per unit time, v is the volume per water molecule, and ρ is the nanopore

density in the NPG membrane. The water permeability, A_m , was then computed from the water flux as

$$A_m = \frac{\phi}{\Delta P - \Delta \Pi}. \quad (2)$$

In Eq. (2), the osmotic pressure difference $\Delta \Pi$ must reflect the salinity at the membrane surface, which is typically greater than the bulk salinity in the feed due to concentration polarization.¹⁶ Because the feed piston is placed less than 10 nm away from the membrane, the feed salinity was approximately uniform during the simulations (see Fig. S1 in the supplementary material¹⁸), ensuring that it is appropriate to calculate $\Delta \Pi$ based on the bulk feed salinity in our system.

III. RESULTS

For each run, we calculated the number of water molecules on the feed side as a function of time. Typical results for $P = 29$, 146, and 1460 bars, respectively, are shown in Figure 2(a). The curves indicate that water molecules permeate across the membrane at a relatively constant rate, and that the flow of water increases monotonically with applied pressure. For $P = 29$ bars, the net driving pressure is only $(\Delta P - \Delta \Pi) = 22$ bars and the slope of curve is correspondingly small. Multiple simulations at the same pressure (not shown in figure) help to reduce the standard error in the flux, even though the relative error in the slope is relatively large compared with runs at higher pressures. For $P = 146$ bars and $P = 1460$ bars, respectively, the net driving pressure is significantly greater and the flow of water molecules is correspondingly larger.

The water flux as a function of pressure is shown in Figure 2(b). The figure indicates that the water flux scales linearly with applied pressure, and the inset in the figure shows that the data at low pressure ($0 < P < 150$ bars) continue to scale linearly with P . We estimated the water permeability of the membrane by calculating the slope in Figure 2(b) using the weighted least squares method. If the nanopore density is assumed to be $1/(24 \text{ \AA})^2 = 1.7 \times 10^{13} \text{ cm}^{-2}$, as in our earlier work, the resulting permeability of NPG is $1041 \pm 20 \text{ l/m}^2\text{-h-bar}$. This compares favorably with our earlier prediction of $1067 \text{ l/m}^2\text{-h-bar}$, or equivalently $40 \text{ l/cm}^2\text{-day-MPa}$.⁹ The data in Figure 2 also contain information about the osmotic pressure of the feed. The transmembrane flux is expected to reach zero when $(\Delta P - \Delta \Pi) = 0$, or $P = P_p + \Delta \Pi \approx 7$ bars. Thus, we would expect the linear fit in Figure 2(b) to cross the x -axis at $P = 7$ bars. In fact, the crossover occurs at $P = 15$ bars, with a standard error of 20 bars. To make sense of the large relative uncertainty associated with this measurement, we note that the motion of water molecules becomes increasingly governed by random diffusion for vanishingly small net driving pressures, which means that the signal-noise ratio from the MD simulations becomes small as $(\Delta P - \Delta \Pi) \rightarrow 0$. We conclude that the MD simulations performed here are not an optimal method for estimating the osmotic pressure with good precision, even when each data point builds on up to 100 ns of total simulation time, as is the case here. Fortunately, we are primarily concerned with the water permeability of the NPG membrane, and the MD simulations are much

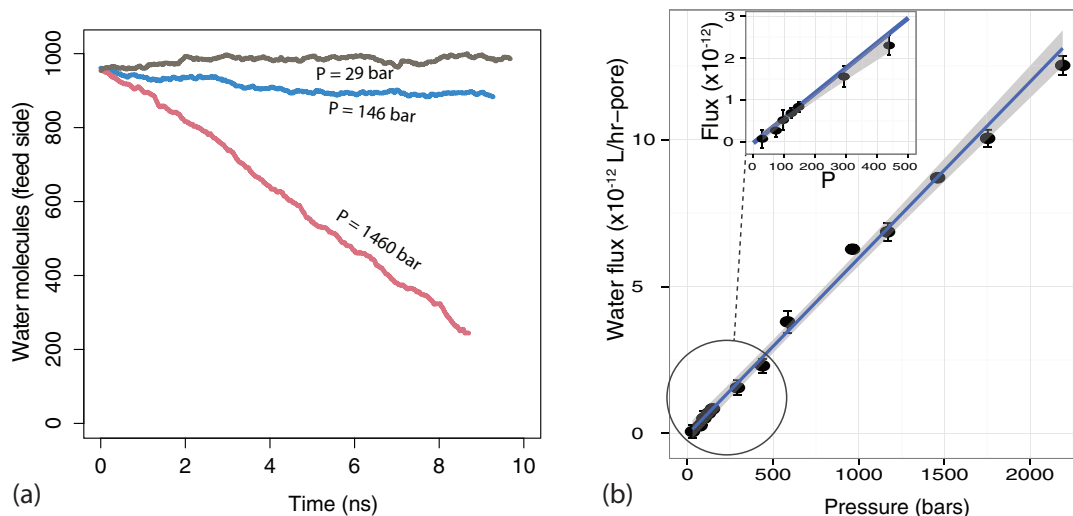


FIG. 2. (a) Number of water molecules on the feed side as a function of simulation time for typical runs at pressures $P = 29$ bars (grey), $P = 146$ bars (blue), and $P = 1460$ bars (red). Although the roughly linearly slopes indicate that flow (water passage per unit time) is approximately constant in both cases, the signal-noise ratio increases with P . (b) Calculated water flux through NPG as a function of applied feed pressure. At realistic pressures for RO desalination ($P < 100$ bars), the flux continues to scale linearly with pressure. Inset shows the water flux for $P < 500$ bars, and the blue line indicates the same linear fit as the main plot. The shaded band in the inset represents a smoothed mean with 99% confidence.

better suited for estimating this quantity: the relative standard error in the permeability is only 2%. An examination of the density of ions as a function of distance from the membrane (see the supplementary material¹⁸) also reveals that concentration polarization is not present at the lengthscale of our simulation, meaning that the net driving pressure is not significantly greater than that predicted from the salt concentration in the bulk.

Finally, we examine the effect of pressure on the permeation of water molecules in the vicinity of the nanopore. A key physical difference between driving water across NPG at $\Delta P = 10$ –100 bars compared with $\Delta P \approx 1000$ bars is how the pressure may affect the force of water molecules on the functional groups at the pore edge. In particular, it may have been expected that higher pressure would lead to greater deformation of the nanopore edge, which could result in a nonlinear increase in flux with increasing pressure. However, our molecular simulations indicate that this is not the case within the pressure range investigated. We have computed the density isosurface of water oxygen atoms for both relatively low (122 bars) and relatively high (1460 bars) pressure

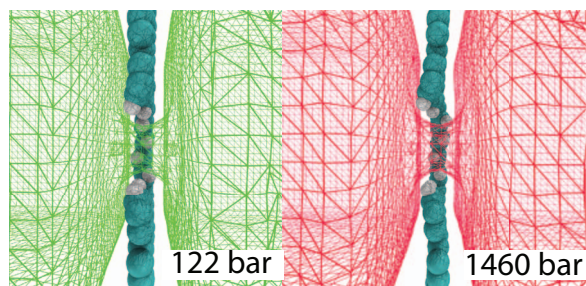


FIG. 3. Comparison of oxygen density maps for $\Delta P = 122$ bars (left) and $\Delta P = 1460$ bars (right). The oxygen density is represented by a wireframe map and is averaged over 10 ns. The figure shows that the density of water molecules in the vicinity of the nanopore is similar for high vs. low transmembrane pressures.

(see Figure 3). Although the figure indicates that marginally greater pore deformation occurs at high pressure (as seen by the greater deviation of hydrogen atoms from the basal plane of the membrane), the diameter of the oxygen density map inside the pore is unchanged compared with the low pressure case. We note that the effect of applied pressure on pore deformation is also affected by the specific functional groups at the pore edge; one would expect a greater degree of deformation in the case of hydroxyl groups or larger functional groups.

In conclusion, we have shown that NPG continues to exhibit ultra-high water permeability at hydraulic pressures employed in RO systems. We showed that the water flux through each nanopore continues to scale linearly with applied pressure, with a slope of $6.0 \text{ l/m}^2\text{-bar-pore}$, corresponding to a water permeability of $\sim 10^3 \text{ l/m}^2\text{-h-bar}$ assuming a pore density of $1.7 \times 10^{13} \text{ cm}^{-2}$. We note, however, that the actual water permeability of an NPG membrane will scale linearly with its nanopore density, which may be either lower or higher than $1.7 \times 10^{13} \text{ cm}^{-2}$. By means of comparison, the maximum density that Holt *et al.* were able to achieve in synthesizing double-walled carbon nanotube membranes was $2.5 \times 10^{11} \text{ cm}^{-2}$.¹⁷ Assuming this pore density instead, the water permeability of NPG would be $15 \text{ l/m}^2\text{-h-bar}$, which is still an order of magnitude greater than in commercial thin-film composite (TFC) membranes. We also note that the water permeability reported here is in the absence of concentration polarization, since the accumulation of salt near the membrane affects the permeate flux but is a function of flux rather than an inherent property of the membrane material and also because the implications of concentration polarization in NPG have been explored elsewhere.³

Furthermore, we found that the flexibility of the graphene membrane, which had not been taken into account until now, does not adversely affect the permeability of NPG. While higher pressures do lead to greater deformation at the

nanopore edge, this does not have a significant effect on the flow of water across the nanopores. This study did not investigate the potential for long-range membrane strain. This effect, if it exists, would occur at the lengthscale of hundreds of nanometers due to the morphology of the substrate material. Given that each periodic cell in our simulation comprised a single nanopore, such an investigation lies outside of the scope of the present work. Further work should therefore be aimed at understanding the effect of hydraulic pressure on the mechanical properties of NPG and its implications for this material's desalination performance. Finally, although the purpose of this work was not to examine effects of pressure on salt rejection, it should be noted that no salt permeation was observed in any of the simulations. This strengthens the hypothesis that NPG would be a high-performing membrane for RO desalination.

ACKNOWLEDGMENTS

We thank Athma Pai and Shreya Dave for insightful conversations, as well as the Doug C. Spreng Fund, the Deshpande Center, the NSF Graduate Research Fellowship Program, and the Martin Family Sustainability Fellowship for funding. We gratefully recognize NERSC for computational resources.

- ¹L. Addams, G. Boccaletti, M. Kerlin, M. Stuchtey, W. R. Group, and McKinsey and Company, Charting Our Water Future: Economic Frameworks to Inform Decision-Making, 2030 Water Resources Group, 2009.
- ²M. Elimelech and W. A. Phillip, *Science* **333**, 712 (2011).
- ³D. Cohen-Tanugi, R. K. McGovern, S. H. Dave, J. H. Lienhard, and J. C. Grossman, *Energy Environ. Sci.* **7**, 1134 (2014).
- ⁴L. Liu and X. Chen, *ChemPhysChem* **14**, 2413 (2013).
- ⁵F. Fornasiero, H. G. Park, J. K. Holt, M. Stadermann, C. P. Grigoropoulos, A. Noy, and O. Bakajin, *Proc. Natl. Acad. Sci. U.S.A.* **105**, 17250 (2008).
- ⁶S. Lin and M. J. Buehler, *Nanoscale* **5**, 11801 (2013).
- ⁷T. Humplik, J. Lee, S. C. O'Hern, B. A. Fellman, M. A. Baig, S. F. Hassan, M. A. Atieh, F. Rahman, T. Laoui, R. Karnik, and E. N. Wang, *Nanotechnology* **22**, 292001 (2011).
- ⁸C. Y. Tang, Y. Zhao, R. Wang, C. Hélix-Nielsen, and A. G. Fane, *Desalination* **308**, 34 (2013).
- ⁹D. Cohen-Tanugi and J. C. Grossman, *Nano Lett.* **12**, 3602 (2012).
- ¹⁰W. Humphrey and A. Dalke, *J. Mol. Graphics* **14**, 33 (1996).
- ¹¹S. Plimpton, *J. Comput. Phys.* **117**, 1 (1995).
- ¹²S. J. Stuart, A. B. Tutein, and J. A. Harrison, *J. Chem. Phys.* **112**, 6472 (2000).
- ¹³W. L. Jorgensen, J. Chandrasekhar, J. D. Madura, R. Impey, and M. L. Klein, *J. Chem. Phys.* **79**, 926 (1983).
- ¹⁴J. Zielkiewicz, *J. Chem. Phys.* **123**, 104501 (2005).
- ¹⁵M. Thomas and B. Corry, "Thermostat choice significantly influences water flow rates in molecular dynamics studies of carbon nanotubes," *Microfluid. Nanofluid.* (published online).
- ¹⁶E. Hoek, A. S. Kim, and M. Elimelech, *Environ. Eng. Sci.* **19**, 357 (2002).
- ¹⁷J. K. Holt, H. G. Park, Y. Wang, M. Stadermann, A. B. Artyukhin, C. P. Grigoropoulos, A. Noy, and O. Bakajin, *Science* **312**, 1034 (2006).
- ¹⁸See supplementary material at <http://dx.doi.org/10.1063/1.4892638> for additional plots and methodological suggestions for suitable replicability.